Fabrication of quasi-2D shape-tailored microparticles using wettability contrast-based platforms

Mafalda D. Neto[1], Aukha Stoppa[1,2], Miguel A. Neto[1], Filipe J. Oliveira[1], Maria C. Gomes[1], Aldo R. Boccaccini[2], Pavel A. Levkin[3], Mariana B. Oliveira[1,], João F. Mano[1,*]*

[*]Correspondence: M.B. Oliveira: mboliveira@ua.pt; J.F. Mano: jmano@ua.pt

[1]*Department of Chemistry, CICECO – Aveiro Institute of Materials. University of Aveiro. Campus Universitário de Santiago. 3810-193 Aveiro, Portugal*

[2]*Institute of Biomaterials, Department of Materials Science and Engineering, University of Erlangen-Nuremberg, 91058 Erlangen, Germany*

[3]*Karlsruhe Institute of Technology, Institute of Biological and Chemical Systems (IBCS-FMS), Hermann-von-Helmholtz Pl.1, 76344 Eggenstein-Leopoldshafen, Germany*

Keywords: ultrathin microparticles, quasi-2D nanostructures, oleophobic patterned surfaces, wettable-dewettable contrast, bioinspired surfaces

Abstract

The ability to fabricate materials with ultrathin architectures enabled the breakthrough of low dimensional structures with high surface area that showcase distinctive properties from their bulk counterparts. Those have been exploited in a wide range of fields, including energy harvesting, catalysis, and biomedicine. Despite such versatility, the fine tuning of the lateral dimensions and geometry of these structures remains challenging. Pre-patterned platforms gained significant attention as enabling technologies to process materials with highly controlled shapes and dimensions. Herein, different nanometer-thick particles of various lateral sizes and geometries (e.g., squares, circles, triangles, hexagons) were processed with high precision and definition, resorting to wettability contrast of oleophilic-oleophobic patterned surfaces. Quasi-2D polymeric microparticles with high shape- and size-fidelity could be retrieved as freestanding objects in a single step. These structures showed cell-mediated pliability, and their integration in gravity-enforced human adipose-derived stems cells spheroids led to an enhanced metabolic activity and a modulated secretion of pro-angiogenic factors.

Ultrathin architectures have gained increasing attention for the development of technologies in numerous fields, which has brought into focus the design of low-dimensional structures composed of a myriad of materials, including polymers. Owing to their reduced thickness, the physical and chemical properties of extremely thin materials are amenable to be modulated in a high portion of the whole material itself. This principle has been applied to design materials that outperform the ones processed using bulk architectures, such as spherical particles.[1] The most exploited property of ultrathin materials is their high aspect ratio and high surface area-to-volume ratio. Owing to their maximized surface area and possibility of exposing an abundant amount of active site moieties,[2] these materials have been adapted for applications that include highly effective sensors and catalytic platforms for the scale-up of reactions. Other applications that benefit from the high surface area of ultrathin materials include scavenging platforms, such as energy harvesting systems,[3] and adsorbents[4] able to effectively capture and isolate contaminants or other species of interest via chemical affinity. Furthermore, the extensive interface displayed by these flat materials can also enable their action as surfactants to stabilize Pickering emulsions, in which a physical barrier between the two immiscible phases prevents droplet coalescence preserving their 'balanced' dispersion within the continuous phase.[5]

The extremely reduced thickness of ultrathin films, ranging from tens to several hundred of nanometers,[1,6] confer them with thickness-dependent behavior, which typically culminates in high flexibility. Such compliant nature can be appealing to many different applications ranging from wearable soft electronics[7] to injectable systems in regenerative medicine strategies, acting as minimally invasive implantation units.[6,8] These highly pliable 'sheets' have also been geometrically reconfigured, through folding or bending, into origami-inspired three-dimensional (3D) assemblies.[9–11] Another particular feature is the possibility of processing them as heterofunctional units, as they present two opposing interfaces amenable to be tailored in order to present asymmetric properties on each side, resulting in different functions.[4,12] Additional potential of ultrathin structures to be used as tissue sealants aimed at replacing surgical sutures may be assigned to their non-covalent adhesiveness.[13] This property is particularly interesting for severely damaged tissues, as in cases of burn wounds, where sutures are

impractical, those may also act as a physical barrier against infections.[14]

Among several techniques to assemble nanometer-level materials, the layer-by-layer (LbL) technology[15] and the Langmuir-Blodgett method[16] are noteworthy, as both systems allow fabricating complex architectures at the molecular level, relying on a variety of interaction chemistries, enabling excellent thickness control in the nanoscale. However, these techniques are time-consuming and require multiple steps. Another methods, such as spin- and dip-coating, may provide simpler and faster ways of assembling freestanding ultrathin structures based on the use of (i) sacrificial layers or (ii) cast/supporting layer techniques, followed by a single step polymer deposition.[17,18] These techniques, however, often limit the control over samples' lateral size at the micrometer-scale and, most relevantly, over their geometry. Approaches based on pre-patterned platforms able to confine deposited solutions offer the potential to control the lateral dimensions of materials, as well as their overall shape.[19,20]

Here, we report the development of monodisperse ultrathin polymeric particles, with several hundred nanometers of thickness and highly controlled micrometer-range lateral sizes (50-500 μm). Freestanding micro-objects assorted with different geometries and sizes were obtained resorting to a high-density microdroplet array of low-surface-tension liquids, exploiting for the first time their contrasting wettability properties to produce detachable objects.[21] We developed an easy and straightforward method to produce highly tailorable freestanding microparticles, which supported cell adhesion and expansion, while tailoring the secreting properties of mesenchymal stem cell spheroids.

Micropatterned surfaces based on the localized control of wettability of organic liquids were prepared as previously described.[21] Those enabled the deposition of polymeric solutions on wettable spots of geometrically defined patterns, surrounded by non-wettable regions. While the latter region repels the liquid or solution, the wettable domains, driven by surface tension, can hold it, such that the contact line of the liquid is pinned along the frame of the patterns.[22] A methodology based on a sequential dip-coating process into two different polymer solutions was developed. While the first deposited polymer acted as a sacrificial layer, the second deposited polymer could be

released as a freestanding structure after solvent drying. The selection of polymers with solubility in different solvents enabled to employ the experimental procedure depicted in **Figure 1**a. In a first step, the pristine pre-patterned surface was immersed in a poly(acrylic acid) (PAA) solution prepared in a mixture of ethanol and water. The surface was then immediately and slowly removed from the solution, allowing the dewetting of PAA solution to occur in the wettable arrayed patterns. Upon solvent evaporation, polymer deposition was observed, with strict confinement within the pattern, and recreating its exact shape. Afterwards, the dip-coating and solvent evaporation processes were repeated using a poly-ε-caprolactone (PCL) solution to build-up the second layer. The stacking of different polymeric layers is possible since the solvent in which PCL was prepared – dichloromethane - is not amenable to solubilize the previously deposited PAA layer. The sequential deposition of both polymers was confirmed through fluorescence microscopy, using a PAA solution loaded with coumarin-6, and a PCL solution with Nile Red (Figure 1a). In order to yield freestanding PCL microparticles, a single trigger event consisting on the immersion of the platform in a solution of sodium hydroxide (1 M NaOH) was employed. Due to the pH responsiveness-driven molecular reconfiguration and further dissolution of PAA, NaOH was effective on promoting the etching of the sacrificial polymer layer,[23,24] leading to the release of PCL microparticles from the glass substrate into the solution. A mild mechanical stimulation, such as agitation or simply creating a flow while pipetting the solution up-and-down, can be applied to speed up the process to few seconds (Movie S1, Supporting Information). The dimension and shape of the dried PCL particles was dictated by the wettable pattern, and thus by the photomask design. Consequently, it was possible to produce both on-chip and freestanding particles with different sizes (ranging from 50 to 500 μm) and geometric shapes, including squares, circles, triangles and hexagons (Figure 1b, Figure S1, Supporting Information). The method allowed the formation of sharp-edged particles, in which the definition of the corners could be maintained even after detachment. Furthermore, to validate the versatility of this technique - polymer-wise -, freestanding polystyrene (PS) and poly-L-lactic acid (PLLA) microparticles were also fabricated (Figure S1, Supporting Information). The same conditions were applied for polymer deposition and detachment as the ones used for PCL particles validation, except in the case of PLLA release. Due to the susceptibility of

the polymer to higher pH values, leading to particle disintegration, a 0.1 M NaOH solution was used.

The morphology and topography of both circular and square particles with lateral sizes of 200 μm, on-chip and freestanding, was performed by 3D optical profilometry analysis. Two different approaches were employed to quantitatively assess the fidelity of the polymer pinning efficiency within the patterned domains and, thus, to evaluate the precision and accuracy of the deposition over the patterns: (i) measurement of the size of the particles: diameter for circles, and side dimension for squares (**Figure 2**a), and (ii) measurement of the shape: roundness for circles, and aspect ratio for squares (Figure 2b).[25] On-chip particles showed over 95% size fidelity for both circles and squares, which indicates that polymer deposition led to the highly accurate recreation of the chemically imprinted pattern. In turn, for the freestanding particles the fidelity score was around 93%, and particle dimensions became more scattered. This dispersion in size may be associated with the NaOH treatment used to detach the particles from the surface, as strong bases may hydrolyze ester bonds, hence, slightly degrading the PCL structure.[26] Similarly, a shape fidelity over 97% was obtained for on-chip particles, while freestanding particles displayed a decrease of less than 3%. This clearly demonstrates the efficiency of the method to produce particles with very precise shapes with well-defined and sharp edges as in the case of the squares (Figure 2c).

The thickness of the materials deposited in the wettable patterns was measured in three different stages: (i) after the deposition and drying of the sacrificial PAA layer, (ii) after the build-up of both polymers (PAA + PCL), and (iii) for the PCL particles alone as freestanding objects. Two distinct regions – edges and center - were measured for these three different conditions, as the deposition of the polymer was not uniformly distributed throughout the individual patterned regions because of the coffee ring effect. Initially, the thickness profile of polymer solutions within the patterned domains was convex due to liquid droplet morphology. Conversely, upon solvent evaporation the profile displayed a concave morphology. This phenomenon is known as the coffee-ring-like effect and describes how the evaporation of the droplet occurs, and how it influences polymer deposition. An enhanced evaporation rate is observed at the droplet edge, which leads to an outward flow of the solvent, driving the movement of solutes

towards the contact line and creating a ring-shaped deposition.[27] For the analysis presented here, an approximate average particle thickness was considered and calculated as the arithmetic mean between the maximum value found within the edges and the minimum value in the center. In the case of PAA deposition, the measured thickness is significantly higher ($p < 0.0001$) for squares (ca. 80 nm) comparatively with circles (ca. 60 nm) (Figure 2d). This substantial change can be explained by the differences in the area exhibited by both patterned geometries. The area displayed by the square patterns is higher than the circular ones, thus, square patterns have the capacity to hold a larger droplet, therefore containing more solute. Concerning the deposition of PCL over the sacrificial layer, three different concentrations - 2%, 3.5%, 5% (w/v) - were used. A general tendency shows that particles' thickness increased with the increase in polymer concentration, both for circular and square geometries (Figure 2e). Moreover, the morphology of the microparticles displayed a decrease of the coffee-ring effect with increasing PCL concentration. The interval in thickness ranged from ca. 100 nm up to ca. 300 nm, for the lowest and highest PCL concentration, respectively. Therefore, both thickness and topography can be tailored by tuning polymer concentration. To evaluate the thickness of the freestanding structures, only 5% (w/v) PCL formulation was considered, as those were the easiest particles to handle and displayed the highest thickness along with a less prominent coffee-ring (Figure 2f). Both square and circle geometries showed an approximate thickness of 200 nm. Moreover, those exhibited polydispersity indexes (PDI) of 0.038 and 0.033 for circles and squares, respectively, revealing a highly monodisperse distribution (Figure 2d-f).[28] The morphology of circles and squares is displayed in Figure 2g. An additional approach based on a sequential dipping strategy was employed to investigate the possibility of further tuning particles' thickness. Two solvents with contrasting solubility for PCL - dichloromethane (high solubility) and acetone (low solubility) - were applied to perform sequential dipping. The growth of the films' thickness showed an inconsistent behavior, as the increase of the number of dipping steps was not fully translated into an increase in thickness (Figure S2, Supporting Information).

The behavior of the freestanding 5% PCL ultrathin films while in contact with cells was explored. Conventional microparticulate systems used for the expansion of

adherent cells often show static geometric properties over time. To test the hypothesis of the microparticles' pliability related to their ultra-thinness, MC3T3-E1 cells were cultured on top of the microparticles (**Figure 3**a i). Those were easily twisted and folded after 24 hours of culture, in a phenomenon solely mediated by cell-surface interactions, and by the flexibility of the supporting object (Figure 3a ii). In a second approach, 30 to 50 PCL ultrathin particles were added to cellular suspensions, which were used to prepare gravity-enforced 3D cell aggregates (Figure 3b i and 3b ii). Such kind of assemblies are in line with bottom-up strategies of producing hybrid tissues that could be used for biomedicine, including tissue engineering.[29,30] Both, all-cellular hASCs aggregates, as well as microparticle-containing aggregates, showed identical diameters: 469 $\pm$ 33 μm and 491 $\pm$ 48 μm, respectively, at day 1, decreasing about 20% of their original size at day 3 (Figure 3 iii). The decrease in spheroid diameter was probably related to spheroids contraction, which led to increasing compactness overtime, culminating in a more circular morphology overtime (Figure S3, Supporting Information). The addition of microparticles to hASCs aggregates did not compromise the formation of cellular spheroids with typical shape and morphology. The hydrophilization of PCL microparticles by the NaOH treatment exposed carboxylated groups at the surface, increasing its surface energy, necessary for cells to adhere.[26] Upon cell adherence and spheroid formation, the particles are effortlessly twisted by the cells due to their ultra-thinness and not-stiff morphology. The cross-section of the spheroids (Figure 3b iv) depicts a moderate roughness in the interior of both control and microparticle-containing conditions, seemingly caused by densely packed cells during spheroid compaction. Throughout the inner surface of the microparticle-loaded spheroid, quasi-transparent structures, which were here identified as microparticles, could be observed throughout the whole aggregate. The Live/Dead staining of the spheroids (Figure S4 a, Supporting Information) unveiled that the outer-layer cells remained viable both at day 1 and 3, independently of the presence of particles within the cell aggregate. Due to the insufficient oxygen diffusion and nutrient exchange with the medium, both spheroids exhibit an overly developed necrotic core. Nonetheless, inspecting the metabolic activity (Figure 3b v), cells remained metabolically active in both conditions and, at day 3, this activity showed a 2-fold increase ($p < 0.05$) for spheroids containing particles. The fluorescent labeling of the sheet-like particles

allowed their identification through confocal microscopy in particle-containing spheroids (Figure 3b vi). The cross-section of the aggregate revealed embedded particles throughout the whole core of the structure, possibly wrapping up cells. Spheroids with particles also showed higher levels of VEGF released from hASCs (Figure 3b vii) when compared to cell spheroids alone. Although VEGF secretion decreased from day 1 to day 3 in both conditions, particle-free aggregates exhibited a more abrupt decline of 76% ($p<0.05$), whereas aggregates incorporating particles showed 50% of decrease (non-significant), disclosing that the incorporation of particles into hASCs spheroids had a positive effect on prolonging and supporting the continuously release of the soluble factor over time. Solely in the presence of bare and non-functionalized PCL particles, the performance and secretion profile of hASCs was modulated without the need of any additional cell behavioral influencers. These findings reveal that these structures may be explored as potential pro-angiogenic structures.[31] β1-integrin has been reported to modulate cell function seeded onto biomaterials with different surface chemistries (including NH_2- and OH-rich surfaces[32]) and also to be involved in promoting VEGF secretion through MAPK/ERK signaling pathway[33]. We hypothesized that the incorporation of particles within the cellular structure would potentiate and activate stronger β1-integrin-mediated interactions by introducing an OH-rich and high surface-area material into the construct. In this sense, we hypothesized that by blocking β1-integrin, part of cell-ECM (and possibly cell-microparticles) binding would be impaired, which could give us insight about the role of these interactions in the mediation of VEGF release. Although blocking β1-integrin on hASCs prior to spheroid formation led to a systematic decrease on secreted VEGF, this trend was not statistically significant in any of the studied timepoints (Table S5, Supporting Information). Moreover, the decrease observed for both microparticle-containing and microparticle-free spheroids was similar, indicating that either β1-integrin does not significantly mediate hASCs-microparticle adhesion, or that this effect does not directly correlate with VEGF secretion. Importantly, even when blocked for β1-integrin, hASCs incorporated the microparticles in the structure of the spheroid. To further investigate the role of microparticles in the secreting properties of the spheroids, structures containing a lower mass of microparticles (represented as PCL<) were prepared. Interestingly, a reduction

of microparticle mass by half led to the same effect on VEGF secretion when compared to spheroids containing a higher mass of particles (Table S5, Supporting Information). We hypothesize that the maintenance of VEGF secretion on cell aggregates after 3 days of culture may rely on the role of microparticles as providers of hypoxic cues - well-reported to induce the secretion of VEGF in hASCs[34] - due to their high and probably oxygen-impermeable surface area[35].

In summary, we demonstrate the fabrication of sheet-like microparticles encompassing a vast array of geometries with high precision, high throughput and definition, using a straightforward and scalable method. The technique is compatible with different types of materials, either for the sacrificial or the freestanding "to be" layers. Moreover, the overall thickness of the freestanding particles could be controlled by varying polymer concentration. Gravity-enforced spheroids containing these quasi-2D cell-deformed pliable particles show enhanced metabolic activity, without hindering the typical spheroid formation, morphology and morphometric features. The formed cell-particle structures could also act as a platform for the release of angiogenic factors. Besides their potential application as highly reactive surfaces in green chemistry and energy harvesting approaches, these geometrically controlled ultrathin microparticles may act as valuable elements in the design of "low-biomaterial" living structures, which may integrate human tissue for therapies or disease models - through the tailoring of their physicochemical and geometrical features to drive specific cell functions, possibly through the modulation of cell-mediated folding patterns.[36]

Supporting Information

Supporting Information is available from the Wiley Online Library or from the author.

Acknowledgments

This work was financially supported by the European Research Council grant agreement ERC-2014-ADG-669858 (project ATLAS), by the Programa Operacional Competitividade e Internacionalização, in the component FEDER, and by national funds (OE) through FCT/MCTES, in the scope of the projects 'TranSphera' (PTDC/BTM-

ORG/30770/2017). This work was also developed within the scope of the project CICECO-Aveiro Institute of Materials, UIDB/50011/2020 & UIDP/50011/2020, financed by national funds through the FCT/MEC and when appropriate co-financed by FEDER under the PT2020 Partnership Agreement. Confocal image acquisition was performed in the LiM facility of iBiMED, a node of PPBI (Portuguese Platform of BioImaging): POCI-01-0145-FEDER-022122. M.B. Oliveira knowledges the individual contract CEECIND/03605/2017.

References

[1] W. Zhang, J. Yu, H. Chang, *J. Mater. Chem. B* **2015**, *3*, 4959.

[2] J. Kim, A. S. Campbell, B. E. F. de Ávila, J. Wang, *Nat. Biotechnol.* **2019**, *37*, 389.

[3] S. Lee, B. Yeom, Y. Kim, J. Cho, *Nano Energy* **2019**, *56*, 1.

[4] P. Wang, J. Liu, X. Chen, X. Ma, D. Guo, Z. Li, J. Pan, *Chem. Eng. J.* **2019**, *369*, 793.

[5] M. Inam, J. R. Jones, M. M. Pérez-Madrigal, M. C. Arno, A. P. Dove, R. K. O'Reilly, *ACS Cent. Sci.* **2018**, *4*, 63.

[6] V. Pensabene, S. Taccola, L. Ricotti, G. Ciofani, A. Menciassi, F. Perut, M. Salerno, P. Dario, N. Baldini, *Acta Biomater.* **2011**, *7*, 2883.

[7] S. Chen, S. Peng, W. Sun, G. Gu, Q. Zhang, X. Guo, *Adv. Mater. Technol.* **2019**, *4*, 1800681.

[8] T. Fujie, Y. Mori, S. Ito, M. Nishizawa, H. Bae, N. Nagai, H. Onami, T. Abe, A. Khademhosseini, H. Kaji, *Adv. Mater.* **2014**, *26*, 1699.

[9] Y. Liu, J. Genzer, M. D. Dickey, *Prog. Polym. Sci.* **2016**, *52*, 79.

[10] G. Huang, Y. Mei, *Small* **2018**, *14*, 1703665.

[11] S. J. P. Callens, A. A. Zadpoor, *Mater. Today* **2018**, *21*, 241.

[12] T. Yin, Z. Yang, M. Lin, J. Zhang, Z. Dong, *Chem. Eng. J.* **2019**, *371*, 507.

[13] Y. Okamura, K. Kabata, M. Kinoshita, D. Saitoh, S. Takeoka, *Adv. Mater.* **2009**, *21*, 4388.

[14] Y. Okamura, K. Kabata, M. Kinoshita, H. Miyazaki, A. Saito, T. Fujie, S. Ohtsubo, D. Saitoh, S. Takeoka, *Adv. Mater.* **2013**, *25*, 545.

[15] J. Borges, J. F. Mano, *Chem. Rev.* **2014**, *114*, 8883.

[16] H. Endo, Y. Kado, M. Mitsuishi, T. Miyashita, *Macromolecules* **2006**, *39*, 5559.

[17] T. Fujie, *Polym. J.* **2016**, *48*, 773.

[18] S. Taccola, A. Desii, V. Pensabene, T. Fujie, A. Saito, S. Takeoka, P. Dario, A. Menciassi, V. Mattoli, *Langmuir* **2011**, *27*, 5589.

[19] J. E. C. And, W. T. S. Huck, *Langmuir* **2007**, *23*, 1569.

[20] S. P. R. Kobaku, G. Kwon, A. K. Kota, R. G. Karunakaran, P. Wong, D. H. Lee, A. Tuteja, *ACS Appl. Mater. Interfaces* **2015**, *7*, 4075.

[21] W. Feng, L. Li, X. Du, A. Welle, P. A. Levkin, *Adv. Mater.* **2016**, *28*, 3202.

[22] A. I. Neto, K. Demir, A. A. Popova, M. B. Oliveira, J. F. Mano, P. A. Levkin, *Adv. Mater.* **2016**, *28*, 7613.

[23] Y. Gao, W. Xu, M. J. Serpe, *J. Mater. Chem. C* **2014**, *2*, 5878.

[24] T. Swift, L. Swanson, M. Geoghegan, S. Rimmer, *Soft Matter* **2016**, *12*, 2542.

[25] H. Yu, K. P. Lim, S. Xiong, L. P. Tan, W. Shim, *Adv. Healthc. Mater.* **2013**, *2*, 1188.

[26] L. T. B. Nguyen, A. O. O. Odeleye, C. Y. Chui, T. Baudequin, Z. Cui, H. Ye, *Sci. Rep.* **2019**, *9*, 3477.

[27] M. Mirbagheri, D. K. Hwang, *Adv. Mater. Interfaces* **2019**, *6*, 1900003.

[28] M. Danaei, M. Dehghankhold, S. Ataei, F. Hasanzadeh Davarani, R. Javanmard, A. Dokhani, S. Khorasani, M. R. Mozafari, *Pharmaceutics* **2018**, *10*, DOI 10.3390/pharmaceutics10020057.

[29] I. M. Bjørge, I. S. Choi, C. R. Correia, J. F. Mano, *Nanoscale* **2019**, *11*, 16214.

[30] V. M. Gaspar, P. Lavrador, J. Borges, M. B. Oliveira, J. F. Mano, *Adv. Mater.* **2019**, 1903975.

[31] J. Seo, J. S. Lee, K. Lee, D. Kim, K. Yang, S. Shin, C. Mahata, H. B. Jung, W. Lee, S.-W. Cho, T. Lee, *Adv. Mater.* **2014**, *26*, 7043.

[32] B. G. Keselowsky, D. M. Collard, A. J. García, *Proc. Natl. Acad. Sci. U. S. A.* **2005**, *102*, 5953.

[33] Z. Li, W. Wang, X. Xu, K. Kratz, J. Zou, L. Lysyakova, M. Heuchel, A. Kurtz, M. Gossen, N. Ma, A. Lendlein, *J. Mater. Chem. B* **2017**, *5*, 7415.

[34] S. T. Hsiao, Z. Lokmic, H. Peshavariya, K. M. Abberton, G. J. Dusting, S. Y. Lim, R. J. Dilley, *Stem Cells Dev.* **2013**, *22*, 1614.

[35] A. Guaccio, V. Guarino, M. A. A. Perez, V. Cirillo, P. A. Netti, L. Ambrosio, *Biotechnol. Bioeng.* **2011**, *108*, 1965.

[36] M. D. Neto, M. B. Oliveira, J. F. Mano, *Trends Biotechnol.* **2019**, *37*, 1011.

Figures

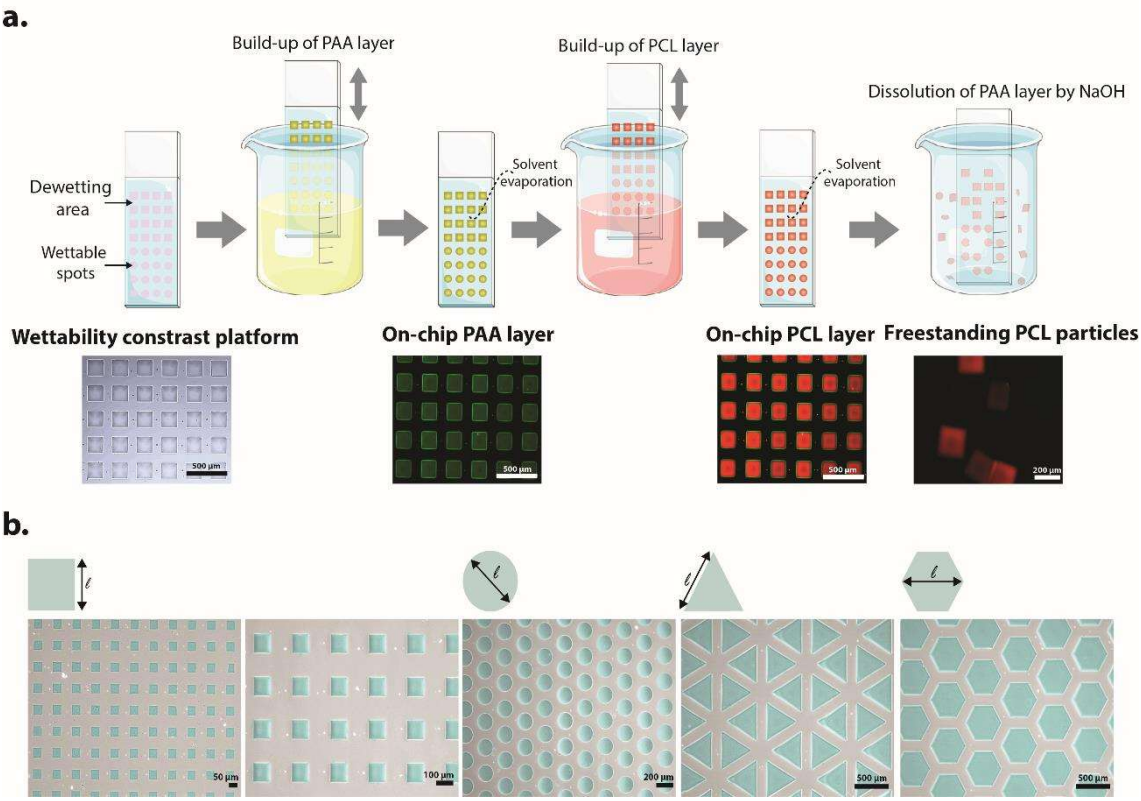

Figure 1. a) Schematic representation of the overall experimental procedure for the fabrication of quasi-2D PCL microparticles. The first step encompasses the dip-coating of the surface in a PAA solution, which upon solvent evaporation and polymer deposition, creates the sacrificial layer. Then, the step is repeated using a PCL solution to form a new top layer. Both polymer solutions were stained with different dyes (PAA with coumarin-6 and PCL with Nile Red) and assessed by fluorescence microscopy to confirm the deposition and correct overlay between the layers. b) Assessing the versatility of the developed platform in generating microparticles portraying different sizes and geometries. Each "ℓ" represented in every image indicates the lateral size defined to measure particle length. All the acquired images were false-colored using Mountains Lab Premium v8.0 software.

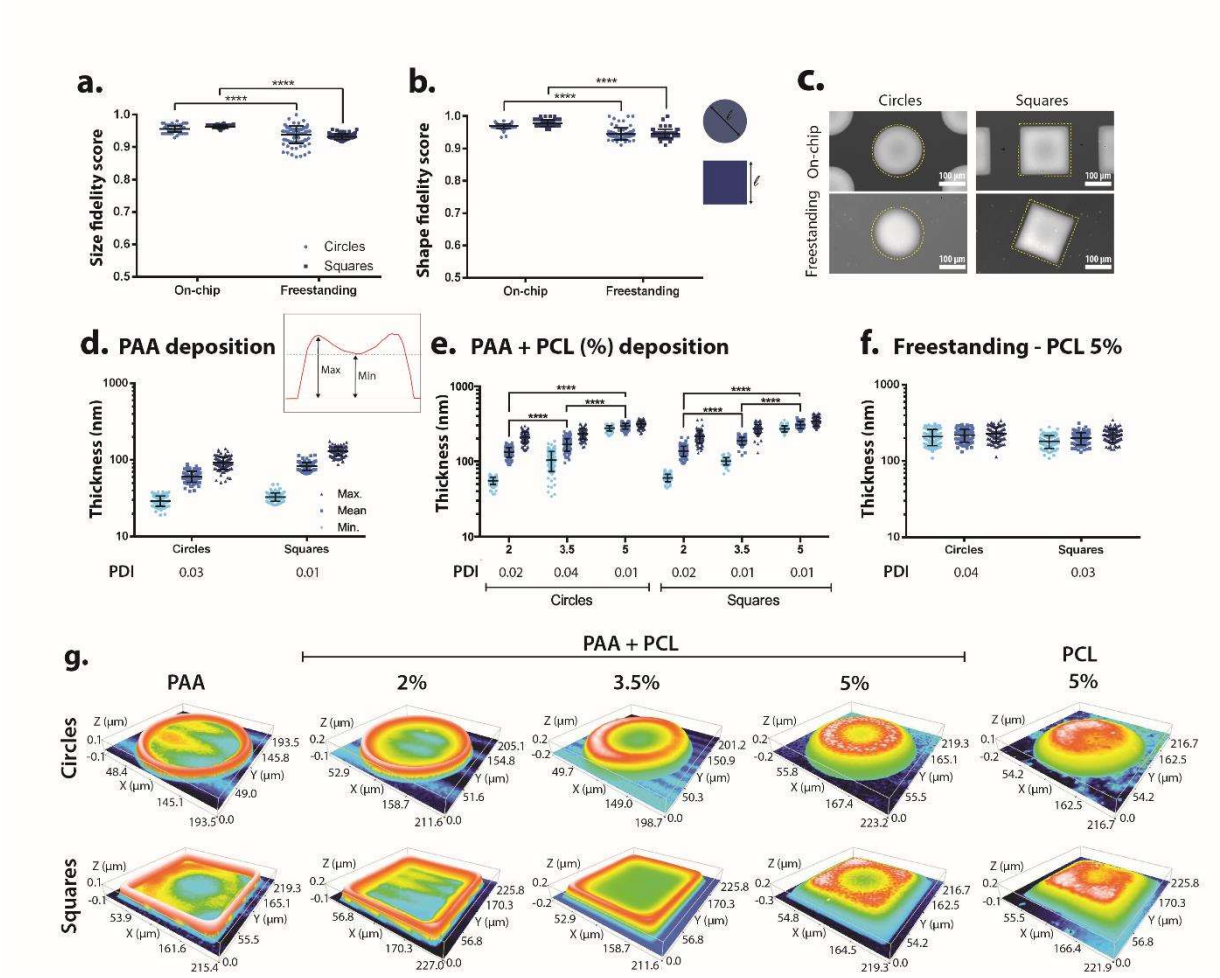

Figure 2. Morphometric characterization and topographic analysis of both circular and square particles (ℓ = 200 μm). a) Size fidelity score of on-chip and freestanding particles. b) Shape fidelity score of on-chip and freestanding particles (roundness of a perfect circle = 1, and aspect ratio of a perfect square = 1) c. Top-views of on-chip and freestanding particles with an overlapping dashed-line shape (yellow) of a perfect ℓ = 200 μm circle and square. d) Thickness of the PAA deposition. The inset represents the estimation of the thickness for all conditions: the mean values were obtained as an arithmetic mean between the maximum and the minimum values. e) Thickness of PAA overlaid with PCL (2%, 3.5%, 5% (w/v)) deposition. f) Thickness of freestanding PCL 5% (w/v) microparticles. A minimum of 75 particles were considered and analyzed per condition. Polydispersity index (PDI) of the thickness measured for all of the conditions indicates that all the particles are highly monodisperse (PDI < 0.05).[28] g) Profilometric views of the on-chip and freestanding particles, revealing the major morphological and topographical differences. For the statistical analysis the data is presented as mean ±

standard deviation (n>75 units) and it is considered statistically different when * $p < 0.05$ and **** $p < 0.0001$.

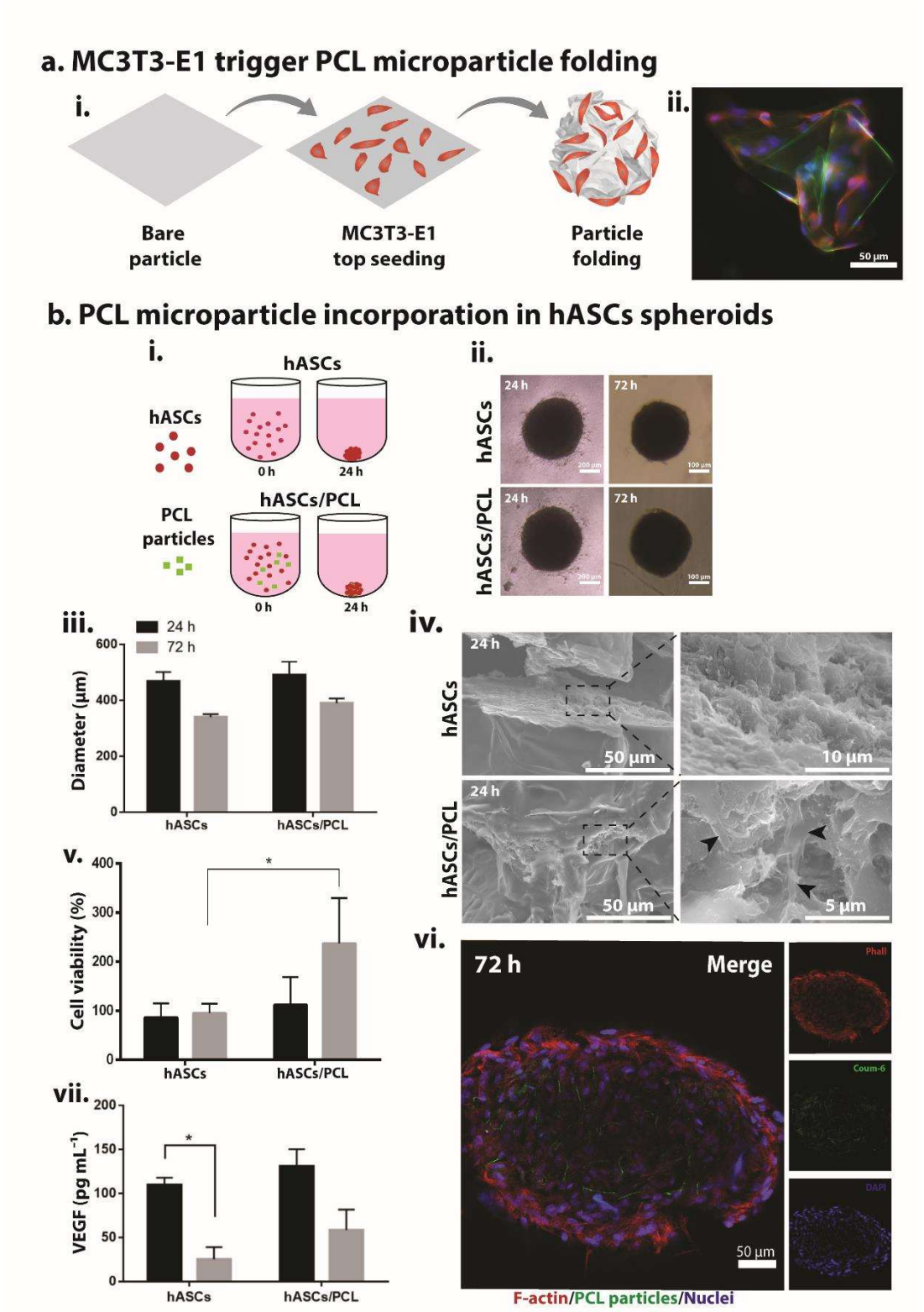

Figure 3. a) MC3T3-E1 trigger PCL microparticle folding and twisting. i) Schematic representation of the cell culture. ii) Fluorescence micrograph of a PCL microparticle